RSC Advances

RSC Publishing

PAPER

View Article Online
View Journal | View Issue

Optical properties of gold particle-cluster core–satellite nanoassemblies†

Cite this: *RSC Advances*, 2013, **3**, 19609

Pyng Yu,*[a] Xiaoming Wen,[b] Yon-Rui Toh,[a] Yu-Chieh Lee[c] and Jau Tang*[ac]

Received 15th May 2013,
Accepted 24th July 2013

DOI: 10.1039/c3ra42388c

www.rsc.org/advances

Better understanding of core–satellite nanostructures is of great interest to researchers owing to their unusual properties and is key to their promising applications. The well-developed techniques based on protein–nanoparticle interactions were adopted to produce core–satellite nanoassemblies of ~10 nm core of Au nanoparticles (AuNPs) covered by Au_{25}@BSA or Au_{10}@histidine nanoclusters (NCs). The photoexcited dynamics in the core–satellite nanoassemblies were studied using steady-state and time-resolved spectroscopic measurements. Fluorescence quenching in AuNP–AuNCs core–satellite nanostructures was observed and confirmed as static quenching. The AuNPs alter neither radiative decay nor nonradiative decay in both nanoclusters. This indicates that the electron/energy transfer within the NP–NCs core–satellite nanoassemblies is absent, in contrast to the results involving other larger NP–NPs core–satellite nanoassemblies.

1. Introduction

Metallic nanomaterials have unique optical properties due to localized surface plasmon resonance (LSPR) and/or discrete energy levels when the size of metal nanoparticles is reduced to a few tens of atoms.[1,2] Tuning of their optical properties can be achieved by chemical assembly of nanoparticles into aggregates or assemblies.[3–7] The LSPR frequency can be finely tuned by controlling the number of nanoparticles, relative orientation of coupled nanoparticles, and interparticle distances.[4] Alivisatos and coworkers produced Au–Ag dimers using DNA linkers and observed plasmon coupling for a single assembly.[5] Recently, Yoon *et al.* developed a method to produce core–satellite nanoassemblies of Au nanoparticles (AuNPs) with well-defined core-to-satellite gap distance by a self-assembled monolayer of alkanedithiol linkers.[6] The resulting nanoassemblies have well-defined structures in which a core AgNPs (50 nm) is covered by an average of 13 nm satellite AuNPs. It was demonstrated that electrons are able to transfer between the particles either by tunneling or through a bridge when the particle separation distance is small enough.[7] Such core–satellite nanoassemblies have been shown to have distinctive optical properties and can be potentially utilized in nanophotonics,[8] surface-enhanced Raman scattering (SERS),[9] bio-sensing and bio-imaging.[10]

Au nanoclusters (NCs), consisting of a few to several tens of atoms with a size smaller than 2 nm, have emerged as a new and fascinating kind of luminescent nanomaterials.[2,11,12] It has been shown that the NCs can exhibit simultaneously atom- (*i.e.* superatom), molecule- and plasmonic nanoparticle-like properties.[13,14] The NCs have high stability since the electronic number fulfills both the closed electron shell rule and geometric factors.[14] As a consequence of enhanced quantum confinement, the fluorescence can emit from the discrete energy levels.[12] These nanoclusters have attracted great interest as they offer potentials for both fundamental research and a wide range of applications, including bio-imaging,[15,16] sensors,[17–19] catalysis,[20,21] hyperthermal therapy,[22] photonics[23] and molecular electronics. Some new photophysical properties have been observed in metallic NCs recently. Temperature dependent experiments showed that electron-electron scattering, rather than electron–phonon interaction, dominates the hot electron relaxation, resulting in a very broad fluorescence in NCs of various sizes.[24,25] On the other hand, the two-state blinking between emissive and dark states of individual Ag_{15}:DNA NCs was demonstrated by Gwinn *et al.* Broad PL spectrum even at low temperature was also proven in ensemble[24] and single nanocluster,[13] which is different from the conventional fluorescent molecules and semiconductor quantum dots. The quantum confined Stark effect was observed in bovine serum albumin (BSA) protected Au_8 and Au_{25} nanoclusters. The study suggests that gold nanoclusters can be a candidate in probing local electric fields and also in pH-sensing in nanoscale environment of biological systems.[26]

The unique properties of nanoclusters are expected to result in distinctive optical properties in metal core–satellite nanoassembly. To our best knowledge, the optical properties

[a]*Research Center for Applied Sciences, Academia Sinica, Taipei, Taiwan. E-mail: pyngyu@gate.sinica.edu.tw; jautang@gate.sinica.edu.tw*
[b]*Australia Centre for Advanced Photovoltaics, University of New South Wales, Sydney 2052, Australia*
[c]*Institute of Photonics, National Chiao-Tung University, Hsinchu, Taiwan*
† Electronic supplementary information (ESI) available. See DOI: 10.1039/c3ra42388c

have not been studied so far in core-satellite assemblies between Au particles and ultrasmall nanoclusters. The aim of this work is to study the photoexcited dynamics in the core-satellite nanoassemblies of ~10 nm AuNPs core covered by Au_{25}@BSA or Au_{10}@histidine NCs satellites. Well-developed protein–nanoparticle interaction techniques were adopted to produce the core–satellite nanoassemblies.[27] Static fluorescence quenching was confirmed in nanoassembly of AuNPs core and Au_{10}@histidine or Au_{25}@BSA NCs satellites, using steady-state and time-resolved spectroscopic measurements. We demonstrated that the electron/energy transfer within the core–satellite nanoassemblies is absent and that is significantly different from the results in the larger nanoparticle satellite reported by Yoon *et al.*[7] The Au NP–NC core–satellite nanoassemblies have potential to be used as a tool to gather information about biochemical systems.[10,28]

2. Experimental section

2.1 Synthesis of Au NCs and Au NPs

The gold NCs used in this study, Au_{10} and Au_{25} which consist of 10 and 25 gold atoms/ions in each nanocluster, were synthesised using a biomineralized approach. Typically, 5 mL of 10 mM $HAuCl_4$ was mixed with 5 mL of 50 mg mL^{-1} bovine serum albumin (BSA, 66.7 kDa) and kept at 37 °C overnight in a incubator while the pH was at 11 for Au_{25} NCs.[29] For Au_{10}@histidine synthesis,[30] 1 mL of 10 mM $HAuCl_4$ was mixed with 3 mL of 0.1 M histidine and kept at 25 °C for two hours in the incubator (*ca.* 250 μM). Citrate capped gold nanoparticles was synthesized using Turkevich approaches.[31] The as-synthesized Au NPs' concentration of 18.9 nM was determined from the absorbance at the maximum and molar extinction of coefficient ($\varepsilon_\lambda = 2.4 \times 10^8$ M^{-1} cm^{-1}).[32]

2.2 Spectroscopic measurements

Absorption and fluorescent spectra were recorded using the JASCO UV/Visible (V-670) and fluorescent (FP-6300) spectrophotometer, respectively. The microsecond (μs) PL lifetimes were measured by the time correlated single photon counting (TCSPC) technique on Microtime-200 (Picoquant). The excitation source is a 467 nm laser with a tunable repetition rate. The femtosecond (fs) time-resolved photoluminescence (TRPL) experiments were performed on an up-conversion fluorimeter (Fluomax, IB Photonics).[33,34] The excitation source is a 400 nm pulsed laser with 100 fs duration and an 80 MHz repetition rate.

3. Results and discussions

It has been shown that Au_{25} NCs comprise 13 neutral Au atoms in the icosahedral core and the semiring which consists of six dimeric –S–Au(I)–S–Au(I)–S– staples. Each Au_{25} NC was completely wrapped and stabilized by the large number thiol group of cysteine in a single BSA.[35] On the other hand, Au_{10}@histidine NCs are composed of Au atoms and stabilized

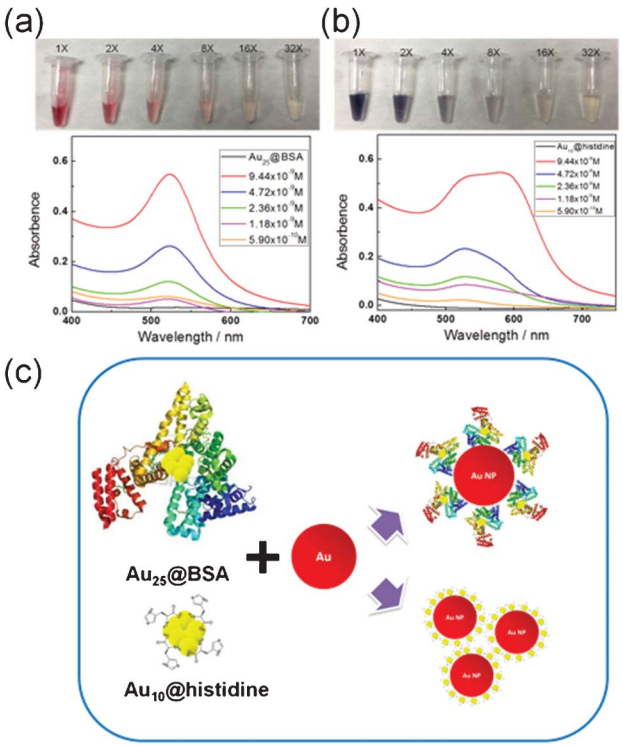

Fig. 1 The photograph and extinction spectrum of (a) Au_{25}@BSA and (b) Au_{10}@histidine mixed with various concentrations of Au nanoparticles. (c) Schematic representation of Au_{25}@BSA and Au_{10}@histidine NCs mixed with Au nanoparticles. The Au_{25}@BSA and Au_{10}@histidine NCs will adsorb onto Au NPs and form core–satellites nanoassemblies. The AuNP–Au_{10}@histidine NCs nanoassemblies will aggregate in the solution.

by the amine group of monolayer histidine.[24] Fig. 1 shows the absorption spectra of Au_{25}@BSA and Au_{10}@histidine NCs mixing various concentrations of AuNPs. The extinction spectra of Au_{25}@BSA NCs and Au_{10}@histidine NCs show a monotonous decrease from UV into the visible and NIR, similar to the bidentate DHLA[36] and PEG[37] protected Au NCs. In contrast, alkylthiol monolayer-protected Au_{25} has unique absorbance peaks.[38] Upon increasing the concentration of AuNPs, the absorption peak of Au NPs' surface plasmon resonance (LSPR) evidently increases around 518.5 nm. When AuNPs mixed with Au_{25}@BSA, the LSPR peak shifts from 518.5 nm to 524 nm because the Au_{25}@BSA NCs can adsorb onto AuNPs and form a core–satellite assembly of nanoparticle-nanoclusters, as shown in Fig. 1c. The LSPR peak of NPs is constant during the entire experimental period, indicating that the mixture is stable with no aggregation. Similarly, Karthikeshwar *et al.* demonstrated the LSPR peak showed a redshift of several nanometers after the Au NPs mixed with BSA due to protein adsorption and without further aggregation within 3 days.[39] Some researchers attributed the interactions between BSA and citrate-reduced Au NPs mainly to the electrostatic interactions between positive charged lysine groups and the negatively charged citrate-coated Au NPs.[40] Many studies showed that the binding constants of BSA and Au NPs were 10^5–10^{11} M^{-1}.[39,41] However, others studies

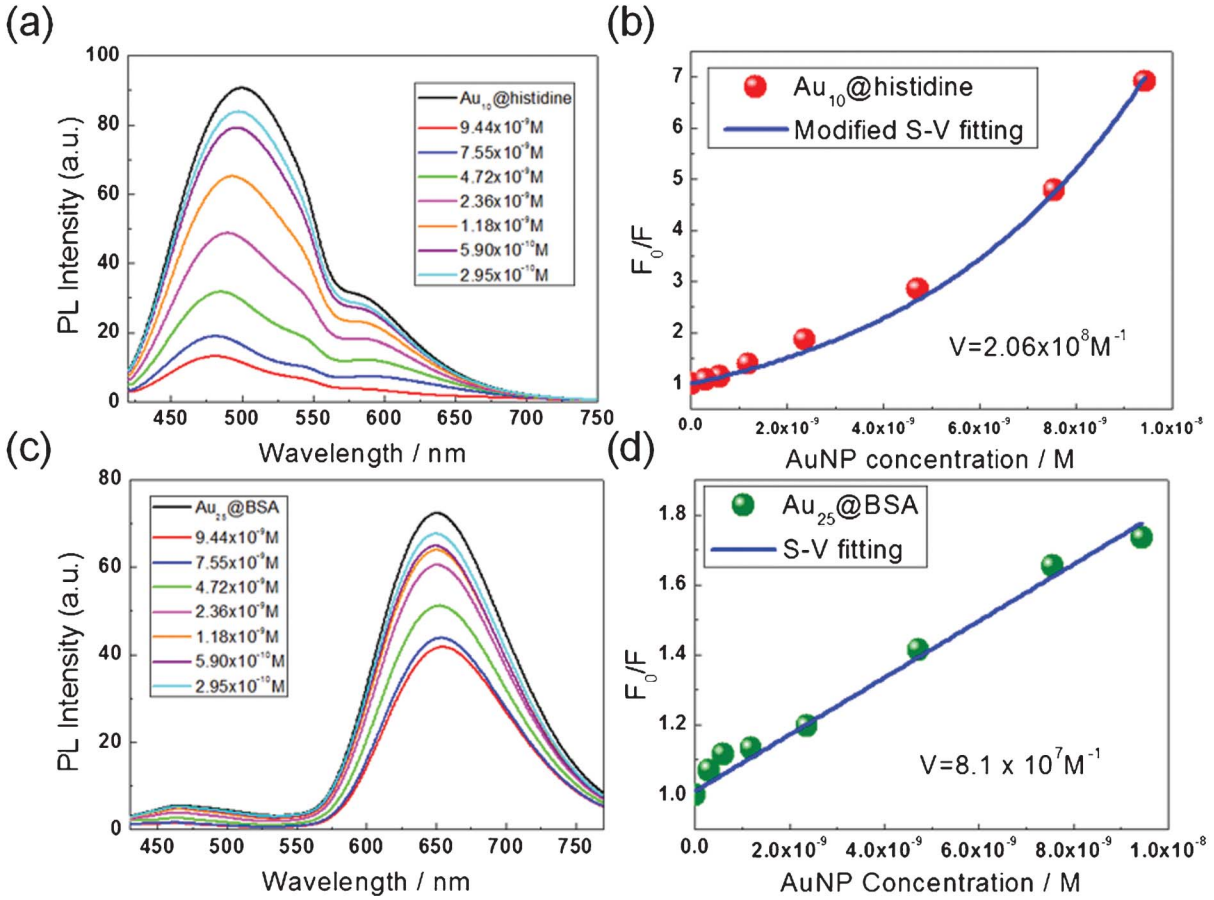

Fig. 2 The fluorescence spectrum of (a) Au_{10}@histidine and (c) Au_{25}@BSA NCs mixed with various concentrations of Au nanoparticles, respectively. The Stern–Volmer plots of (b) Au_{10}@histidine and (d) Au_{25}@BSA NCs corresponding to the peak intensity with various concentrations of Au NPs.

suggested the binding occurs through covalent interactions of cysteine sulfer groups and the Au NP surface.[42] On the other hand, the LSPR peak shifts immediately to longer than 600 nm as soon as the Au NPs were mixed with Au_{10}@histidine NCs, indicating Au_{10}@histidine adsorption will induce aggregation of Au NPs. This is similar to the organothiols induced NP aggregation due to high binding affinities to Au nanoparticles.[39] Fig. 1c schematically shows the core-satellite nanoassemblies through protein-nanoparticle interactions occurring in mixtures of Au_{25}@BSA–AuNPs and Au_{10}@histidine–AuNPs, respectively.

The solutions of Au_{10}@histidine and Au_{25}@BSA NCs exhibit an emission band at 500 nm and 650 nm, respectively. The PL intensity of both Au_{10} and Au_{25} decreases with increasing the concentration of Au nanoparticles ($\sim$10 nm), as shown in Fig. 2a and 2c. A small blue shift of PL peak was observed only in Au_{10}@histidine NCs. The blue shift may arise from the aggregation of nanoparticles which results in reduced polarity in the local environment of the emitting species.[43] In order to obtain the insight into the mechanism of PL quenching, the Stern–Volmer (S–V) plots, the peak intensity as a function of concentration of Au NPs, were shown in Fig. 2b and 2d. It is evident that the plots show linear and upward exponential behavior for Au_{25} and Au_{10} NCs satellite, respectively. In general, for linear S–V behaviour, PL quenching can be arisen from either a dynamic (collisional) or static mechanism. It is well known that dynamic quenching is arisen from the collision between the fluorescent sample and the quencher, whereas the static quenching results from binding between the fluorescent sample and the quencher. In static quenching a complex is formed which has a nonfluorescent ground state. However, the upward curvature of the Stern–Volmer plots here can be attributed to either combined dynamic and static quenching or solely static quenching with a large extent.[44] The latter was usually interpreted in terms of a ''sphere of action'' and described by the modified Stern–Volmer equation:

$$F_0/F = (1 + K_D[Q])\exp([Q]V) \quad (1)$$

where $[Q]$ is the concentration of AuNPs; K_D is the dynamic quenching constant and V is the static quenching constant. In the sphere of action, the apparent static component is due to the quencher being adjacent to the fluorophore at the moment of excitation. These spatially closed fluorophore–quencher pairs are immediately quenched, and are referred to as dark

complexes. It is noteworthy that the fluorophore and quencher do not actually form a ground-state complex. The long range static quenching was observed in P3HT and MWCNT,[45] as well as rhodamine B and CNTs pairs.[46]

To distinguish the static quenching from the dynamic quenching in these experiments one can examine their absorption spectra of the fluorophore.[44] Dynamic quenching only affects the excited states of the fluorophore, and thus no change was expected in the absorption spectra. In contrast, a ground state complex formation (nonfluorescent complex of the fluorophore) will result in perturbation of the absorption spectrum, which shifts the UV absorption maximum and indicates a strong probability of static quenching. Unfortunately, as aforementioned, the absorption of NCs is featureless and hidden by strong plasmon of AuNPs in this experiment. Alternatively, the most definitive method is the PL lifetime measurement. For dynamic quenching, the decrease in lifetime occurs because quenching is an additional relaxation process that depopulates the excited state ($F_0/F = \tau_0/\tau$). On the contrast, the static quenching does not decrease the lifetime because only the fluorescent NCs were observed, and the uncomplexed fluorophores have the unquenched lifetime τ_0. ($\tau_0/\tau = 1$).

To determine the mechanism of the quenching by gold nanoparticles, fluorescence lifetime measurements were carried out using the ultrafast upconversion technique. Firstly, the fluorescence evolution was shown in Fig. 3a in a picosecond (ps) time scale at 500 nm, corresponding to the peak maximum of Au_{10}@histidine NC. A very fast rise was observed, which suggests the transient equilibration of hot electrons *via* electron-electron scattering on the fs time scale. The evolution can be fitted by a three-exponential function and the fitting parameters were listed in Table 1. A sharp decay (τ_1 = 2.98 ps, 84%) is observed with a very large amplitude. In addition, a relatively slow component (τ_2) was observed, 30.0 ps. There are several possible processes responsible for the fast decay: electron–phonon coupling, carrier trapping or Auger recombination.[47] Here, we performed intensity dependent measurements to elucidate the ps decay process (see Fig. S2, ESI†). The Auger recombination could be ruled out since the time constants do not depend on the pump fluence and remain almost constant. Therefore, we proposed the ps decays in Au_{10}@histidine NCs are due to trapping of charges into defect states (τ_1) and the electron-acoustic phonon scattering (τ_2), respectively. In quantum confined Au NCs, it is found that the phonon coupling is significantly weaker than that in nanoparticles.[24,25] Moreover, the slowest component with lifetime >200 ps can be ascribed to the nonradiative recombination (τ_3) and such a slow component was also observed in Au_{11} NCs.[48] The nanosecond fluorescence lifetime of Au_{10}@histidine was further measured by TCSPC technique. Essentially, the lifetime represents the recombination rate of the electron and hole and is determined by their wavefunction overlapping. As shown in Fig. 3b, the fluorescence evolution can be fitted by a biexponential function, which indicates two decay components. The fast one can be ascribed to the nonradiative recombination with lifetime of 600–700 ps, similar to the aforementioned slowest component in ultrafast measurements. The slow component should correspond to the radiative recombination. Table 1 shows that there is no observable change in the Au_{10}@histidine fluorescence decay profile (either ps or ns time scales) at 500 nm before and after addition of AuNPs.

Fig. 4 shows the fluorescence evolution in the ps time scale at 650 nm, corresponding to the peak of Au_{25}@BSA NCs. A very fast rise was observed, which suggests the transient equilibration of hot electrons *via* electron–electron scattering on the femtosecond time scale. The evolution can be fitted by a biexponential function and the fitting parameters are tabulated in Table 2. A sharp decay component of 2.07 ps was observed. Similar to Au_{10} NCs, these ultrafast decays can be attributed to the surface/defect trapping. Moreover, the slow component with lifetime ~30 ps can be ascribed to the electron-acoustic phonon scattering (τ_3).

The microsecond fluorescence lifetime measurements were carried out using the TCSPC technique. The fluorescent

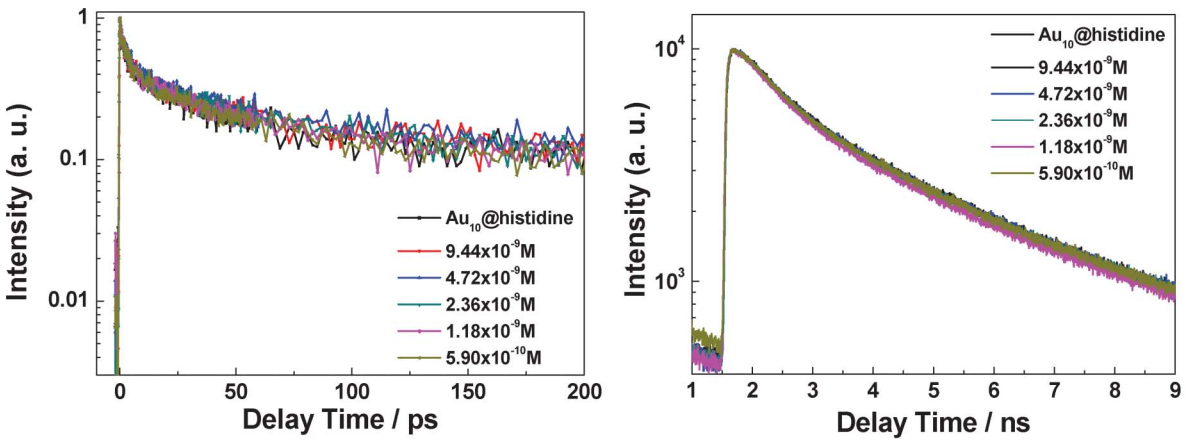

Fig. 3 The fluorescence evolution of Au_{10}@histidine and mixed with various concentrations of Au nanoparticles at 500 nm measured by (a) up-conversion (picosecond time scale) technique and (b) fs-TCSPC technique (nanosecond time scale).

Table 1 Fitting parameters of fluorescence time traces of Au_{10}@histidine and mixed with various concentrations of Au nanoparticles at 500 nm measured by the fs-TCSPC and up-conversion techniques

	Up-conversion			TCSPC	
	τ_1 (ps)	τ_2 (ps)	τ_3 (ps)	τ_1 (ns)	τ_2 (ns)
Au_{10}@histidine	2.98 (84%)	34.38 (12%)	614.13 (4%)	0.67	3.13
[AuNP] = 4.72 × 10^{-9} M	2.99	28.88	265.11	0.69	3.18
[AuNP] = 2.36 × 10^{-9} M	2.67	27.26	235.01	0.67	3.14
[AuNP] = 1.18 × 10^{-9} M	2.41	28.02	267.44	0.69	3.17
[AuNP] = 5.90 × 10^{-10} M	3.09	28.37	247.33	0.66	3.13

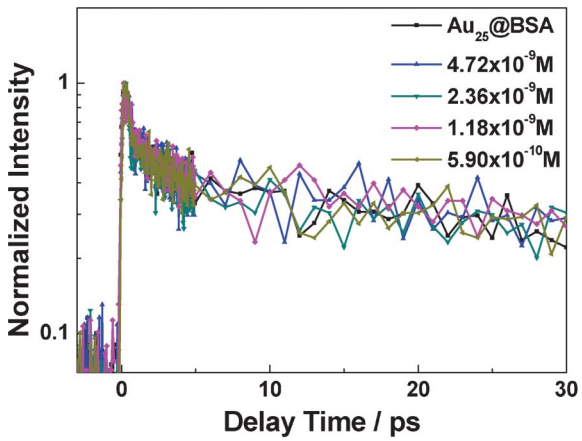

Fig. 4 The fluorescence evolution of Au_{25}@BSA and mixed with various concentrations of Au nanoparticles at 600 nm measured by up-conversion (picosecond time scale) technique.

dynamics of BSA-protected Au_{25} cluster exhibits three decay components: intersystem crossing (ISC, singlet to triplet) and prompt fluorescence (PF) are in the ns scale, and delayed fluorescence (DF) is in the μs scale.[33] Upon excitation of NCs, the excited electrons can recombine with a hole in the singlet state *via* prompt fluorescence or becomes localized in the triplet state through efficient ISC processes. Repopulated electrons from the triplet to singlet state will emit fluorescence with the same spectra with a much longer decay component. In Fig. 5, there were no evident changes of the fluorescence decay profile at various concentrations of AuNPs. The experiment confirms that AuNPs do not alter the lifetimes of both PF and DF decay components. Obviously, all the spectra lie over one another before and after formation of AuNP core and Au_{10}@histidine/Au_{25}@BSA NCs satellites nanoassemblies.

Table 2 Fitting parameters of fluorescence time traces of Au_{25}@BSA and mixed with various concentrations of Au nanoparticles at 600 nm measured by up-conversion and TCSPC measurements

	Up-conversion		TCSPC		
	τ_1 (ps)	τ_2 (ps)	τ_1 (ns)	τ_2 (ns)	τ_3 (μs)
Au_{25}@BSA	1.8 (46%)	28.3 (54%)	1.16	8.05	1.32
[AuNP] = 4.72 × 10^{-9} M	1.8	33.6	1.07	9.11	1.37
[AuNP] = 2.36 × 10^{-9} M	2.3	28.1	1.14	11.4	1.35
[AuNP] = 1.18 × 10^{-9} M	2.1	32.5	1.01	7.97	1.35
[AuNP] = 5.90 × 10^{-10} M	2.6	27.5	1.33	10.4	1.37

The PL decay times remain constant with formation of nanoassemblies, indicating that the contribution of dynamics quenching could be completely ruled out. Therefore, the dynamic quenching constant (K_D) can be negligible in eqn (1); and the quenching process becomes purely static and thus follows simple exponential growth. The static quenching constants are determined as V = 2.06 × 10^8 M^{-1} and 8.10 × 10^7 M^{-1} for Au_{10}@histidine and Au_{25}@BSA NCs satellites, respectively. It is noteworthy that similar static quenching constants derived from the sphere of action model were observed in semiconducting polymer nanoparticles and Au nanoparticles (~10^8 M^{-1}),[49] but are much larger than those reported from Au_8@PAMAM NCs and 2-pyridinethiol (2-PyT) pair, that is, V = 5.0 × 10^2 M^{-1}.[28] According to a sphere of action model, the quenching radius can be obtained from equation:

$$V/N_A = 4\pi r^3/3 \quad (2)$$

where r is the static quenching radius and N_A is Avogadro's number. The quenching radius (r) was estimated to be ~434 nm for AuNP–Au_{10}@histidine core–satellite nanoassemblies, which was 70 times larger than the sum of radii of AuNPs and Au_{10}@histidine (*i.e.* ~6 nm). The value is significant larger than those reported from Au_8@PAMAM NCs and 2-PyT pair, that is, r = 5.8 nm.[28] The large quenching radius implies that the PL quenching can take place while Au NCs and AuNPs are not close to each other. In general, Förster resonance energy transfer (FRET) results from dipole–dipole interactions and the length scale is on the order of maximum 10 nm. Recently, several groups demonstrated that surface energy transfer (NSET) pairs can be used to measure several tens of nanometers distance,[50] and the coupled plasmonic particles rulers have sub-100 nm distance.[51] Therefore, such a large quenching radius seems unreasonable. Instead the upward exponential S–V plot may originate from the aggregation of AuNPs–Au_{10}@histidine nanoassemblies. As the AuNPs concentration increases, the aggregation of nanoassemblies increases the PL quenching, and the sphere of action model is not suitable for this case.

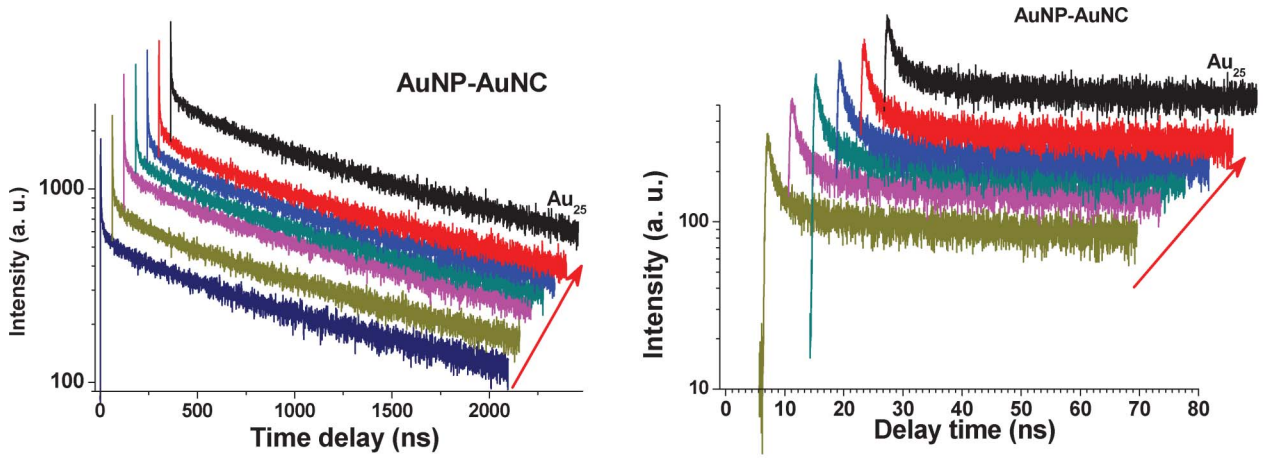

Fig. 5 The fluorescence evolution of Au_{25}@BSA mixed with various concentrations of Au nanoparticles at 650 nm measured by TCSPC technique (nanosecond time scale). Arrow indicates the increase of the concentration of AuNPs.

Recently, Yoon *et al.* studied the plasmon coupling between AgNPs core and AuNP satellites as the core-to-satellite gap distance varies from 2.3 to 0.7 nm.[7] The gap distance of AuNP core and protein wrapped AuNC satellites is estimated to be smaller than 1 nm and a charge transfer was observed at a ~1 nm gap. Ultrafast singlet electron transfer was observed in Au_{25}–PySH system.[52] More recently, effective triplet electron transfer was confirmed in Au_{25}–Hg^{+} system and could be used for a selective and sensitive detection of Hg^{+}.[19] On the other hand, the energy transfer was observed in AuNP–BSA–CdS QD nanoassemblies by Mandal *et al.*[53] From TEM measurements, a short gap distance of ~1.7 nm was confirmed between the QD and Au NPs. In our experiments the interaction between AuNP and AnNC is confirmed as static quenching due to formation of stable core-satellite nanoassembly in which the distance between AuNP core and AuNC satellite is relatively large, most likely owing to the effect of ligands. It should be emphasized that neither charge transfer nor energy transfer occurs within the AuNP–AuNCs nanoassemblies. Apparently, the interaction in the AuNP–AuNC nanoassembly is different from the large NP–NPs nanoassemblies and metal–semiconductor nano-hybrids. We anticipate such AuNP–AuNC nanoassemblies have potential to be used as a tool to gather information about biochemical systems. Further theoretical and experimental studies should be conducted to obtain deeper detailed insight.

4. Conclusions

We have produced the core–satellite nanoassemblies of a ~10 nm AuNPs core covered by Au_{25}@BSA or Au_{10}@histidine NCs satellites using the well-developed protein–nanoparticle interaction techniques. Fluorescence quenching was observed in the core–satellite nanoassemblies of Au_{25}@BSA and Au_{10}@histidine NC–AuNP core. The quenching was confirmed as static quenching due to formation of a dark complex. The large static quenching constants were determined as $V = 2.06 \times 10^{8}$ M^{-1} and 8.10×10^{7} M^{-1} for Au_{25}@BSA and Au_{10}@histidine NC satellites, respectively. We observed experimentally that the AuNPs do not alter either the radiative decay or the nonradiative decay in both Au_{10} and Au_{25} nanoclusters. It is interesting to point out that a unique interaction occurs between AuNP cores and AuNCs by formation of a dark complex. Neither electron transfer nor energy transfer was observed in the core-satellite nanoassemblies. This is apparently different from the results in larger NP–NPs core–satellite nanoassemblies and NP–semiconductor QD nanohybrids.

Acknowledgements

Thanks to Ms. C.-Y. Chien of Precious Instrument Center (National Taiwan University) for the assistance in TEM experiments. The authors acknowledge financial support from Academia Sinica (AS) Nano Program and National Science Council (NSC) of Taiwan under the program 99-2221-E-001-002-MY3 and No.99-2113-M-001-023-MY3.

References

1 K. L. Kelly, E. Coronado, L. L. Zhao and G. C. Schatz, The optical properties of metal nanoparticles: the influence of size, shape, and dielectric environment, *J. Phys. Chem. B*, 2003, **107**(3), 668–677.
2 J. Zheng, P. R. Nicovich and R. M. Dickson, Highly fluorescent noble metal quantum dots, *Annu. Rev. Phys. Chem.*, 2007, **58**, 409.
3 M. R. Jones, K. D. Osberg, R. J. Macfarlane, M. R. Langille and C. A. Mirkin, Templated techniques for the synthesis and assembly of plasmonic nanostructures, *Chem. Rev.*, 2011, **111**(6), 3736–3827.
4 P. K. Jain, S. Eustis and M. A. El-Sayed, Plasmon coupling in nanorod assemblies: optical absorption, discrete dipole

approximation simulation, and exciton-coupling model, *J. Phys. Chem. B*, 2006, **110**(37), 18243–18253.
5 S. Sheikholeslami, Y.-w. Jun, P. K. Jain and A. P. Alivisatos, Coupling of optical resonances in a compositionally asymmetric plasmonic nanoparticle dimer, *Nano Lett.*, 2010, **10**(7), 2655–2660.
6 J. H. Yoon, J. Lim and S. Yoon, Controlled Assembly and Plasmonic Properties of Asymmetric Core–Satellite Nanoassemblies, *ACS Nano*, 2012, **6**(8), 7199–7208.
7 J. H. Yoon, Y. Zhou, M. G. Blaber, G. C. Schatz and S. Yoon, Surface Plasmon Coupling of Compositionally Heterogeneous Core–Satellite Nanoassemblies, *J. Phys. Chem. Lett.*, 2013, **4**, 1371–1378.
8 V. Giannini, A. I. Fernández-Domínguez, S. C. Heck and S. A. Maier, Plasmonic nanoantennas: fundamentals and their use in controlling the radiative properties of nanoemitters, *Chem. Rev.*, 2011, **111**(6), 3888.
9 P. L. Stiles, J. A. Dieringer, N. C. Shah and R. P. Van Duyne, Surface-enhanced Raman spectroscopy, *Annu. Rev. Anal. Chem.*, 2008, **1**, 601–626.
10 Y.-w. Jun, S. Sheikholeslami, D. R. Hostetter, C. Tajon, C. S. Craik and A. P. Alivisatos, Continuous imaging of plasmon rulers in live cells reveals early-stage caspase-3 activation at the single-molecule level, *Proc. Natl. Acad. Sci. U. S. A.*, 2009, **106**(42), 17735–17740.
11 P. L. Xavier, K. Chaudhari, A. Baksi and T. Pradeep, Protein-protected luminescent noble metal quantum clusters: an emerging trend in atomic cluster nanoscience, *Nano Reviews*, 2012, **3**, 14767.
12 R. Jin, Quantum sized, thiolate-protected gold nanoclusters, *Nanoscale*, 2010, **2**(3), 343–362.
13 S. S. R. Oemrawsingh, N. Markesevic, E. G. Gwinn, E. R. Eliel and D. Bouwmeester, Spectral Properties of Individual DNA-Hosted Silver Nanoclusters at Low Temperatures, *J. Phys. Chem. C*, 2012, **116**(48), 25568–25575.
14 M. Walter, J. Akola, O. Lopez-Acevedo, P. D. Jadzinsky, G. Calero, C. J. Ackerson, R. L. Whetten, H. Grönbeck and H. Häkkinen, A unified view of ligand-protected gold clusters as superatom complexes, *Proc. Natl. Acad. Sci. U. S. A.*, 2008, **105**(27), 9157–9162.
15 D. Tian, Z. Qian, Y. Xia and C. Zhu, Gold Nanocluster-Based Fluorescent Probes for Near-Infrared and Turn-On Sensing of Glutathione in Living Cells, *Langmuir*, 2012, **28**(8), 3945–3951.
16 L. Yang, L. Shang and G. U. Nienhaus, Mechanistic aspects of fluorescent gold nanocluster internalization by live HeLa cells, *Nanoscale*, 2013, **5**(4), 1537–1543.
17 L. V. Nair, D. S. Philips, R. S. Jayasree and A. Ajayaghosh, A Near-Infrared Fluorescent Nanosensor (AuC@ Urease) for the Selective Detection of Blood Urea, *Small*, 2013, **9**(16), 2673–2677.
18 J. Xie, Y. Zheng and J. Y. Ying, Highly selective and ultrasensitive detection of Hg^{2+} based on fluorescence quenching of Au nanoclusters by Hg^{2+}–Au^{+} interactions, *Chem. Commun.*, 2010, **46**(6), 961–963.
19 P. Yu, X. Wen, Y. R. Toh, J. Huang and J. Tang, Metallophilic Bond-Induced Quenching of Delayed Fluorescence in Au25@ BSA Nanoclusters, *Part. Part. Syst. Charact.*, 2013.
20 E. Gross, J. H.-C. Liu, S. Alayoglu, M. A. Marcus, S. C. Fakra, F. D. Toste and G. A. Somorjai, Asymmetric catalysis at the mesoscale: Gold nanoclusters embedded in chiral self-assembled-monolayer as heterogeneous catalyst for asymmetric reactions, *J. Am. Chem. Soc.*, 2013, **135**(10), 3881–3886.
21 Y. Tao, Y. Lin, Z. Huang, J. Ren and X. Qu, Incorporating Graphene Oxide and Gold Nanoclusters: A Synergistic Catalyst with Surprisingly High Peroxidase-Like Activity Over a Broad pH Range and its Application for Cancer Cell Detection, *Adv. Mater.*, 2013, **25**(18), 2594–2599.
22 R. S. McCoy, S. Choi, G. Collins, B. J. Ackerson and C. J. Ackerson, Superatom Paramagnetism Enables Gold Nanocluster Heating in Applied Radiofrequency Fields, *ACS Nano*, 2013, **7**(3), 2610–2616.
23 S. Raut, R. Chib, R. M. Rich, D. Shumilov, Z. Gryczynski and I. Gryzcynski, Polarization properties of fluorescent BSA protected Au25 nanoclusters, *Nanoscale*, 2013, **5**, 3441–3446.
24 P. Yu, X. Wen, Y.-R. Toh and J. Tang, Temperature-Dependent Fluorescence in Au10 Nanoclusters, *J. Phys. Chem. C*, 2012, **116**(11), 6567–6571.
25 X. Wen, P. Yu, Y.-R. Toh and J. Tang, Structure-correlated dual fluorescent bands in BSA-protected Au25 nanoclusters, *J. Phys. Chem. C*, 2012, **116**(21), 11830–11836.
26 X. Wen, P. Yu, Y.-R. Toh and J. Tang, Quantum Confined Stark Effect in Au8 and Au25 Nanoclusters, *J. Phys. Chem. C*, 2013, **117**(7), 3621–3626.
27 S. T. Yang, Y. Liu, Y. W. Wang and A. Cao, Biosafety and Bioapplication of Nanomaterials by Designing Protein–Nanoparticle Interactions, *Small*, 2013, **9**(9–10), 1635–1653.
28 T. H. Wu, Y. Y. Hsu and S. Y. Lin, A Redox-Switchable Au8-Cluster Sensor, *Small*, 2012, **8**(13), 2099–2105.
29 J. Xie, Y. Zheng and J. Y. Ying, Protein-directed synthesis of highly fluorescent gold nanoclusters, *J. Am. Chem. Soc.*, 2009, **131**(3), 888–889.
30 X. Yang, M. Shi, R. Zhou, X. Chen and H. Chen, Blending of $HAuCl_4$ and histidine in aqueous solution: a simple approach to the Au_{10} cluster, *Nanoscale*, 2011, **3**(6), 2596–2601.
31 S. S. Shankar, S. Bhargava and M. Sastry, Synthesis of gold nanospheres and nanotriangles by the Turkevich approach, *J. Nanosci. Nanotechnol.*, 2005, **5**(10), 1721–1727.
32 J.-Y. Kim, D. H. Lee, S. J. Kim and D.-J. Jang, Preferentially linear connection of gold nanoparticles in derivatization with phosphorothioate oligonucleotides, *J. Colloid Interface Sci.*, 2008, **326**(2), 387–391.
33 X. Wen, P. Yu, Y.-R. Toh, A.-C. Hsu, Y.-C. Lee and J. Tang, Fluorescence Dynamics in BSA-Protected Au25 Nanoclusters, *J. Phys. Chem. C*, 2012, **116**(35), 19032–19038.
34 P. Yu, X. Wen, Y.-R. Toh and J. Tang, Temperature-Dependent Fluorescence in Carbon Dots, *J. Phys. Chem. C*, 2012, **116**(48), 25552–25557.
35 A. Baksi, P. L. Xavier, K. Chaudhari, N. Goswami, S. Pal and T. Pradeep, Protein-encapsulated gold cluster aggregates: the case of lysozyme, *Nanoscale*, 2013, **5**(5), 2009–2016.
36 L. Shang, N. Azadfar, F. Stockmar, W. Send, V. Trouillet, M. Bruns, D. Gerthsen and G. U. Nienhaus, One-Pot Synthesis of Near-Infrared Fluorescent Gold Clusters for Cellular Fluorescence Lifetime Imaging, *Small*, 2011, **7**(18), 2614–2620.

37 E. Oh, F. K. Fatemi, M. Currie, J. B. Delehanty, T. Pons, A. Fragola, S. Lévêque-Fort, R. Goswami, K. Susumu and A. L. Huston, PEGylated Luminescent Gold Nanoclusters: Synthesis, Characterization, Bioconjugation, and Application to One-and Two-Photon Cellular Imaging, *Part. Part. Syst. Charact.*, 2013, **30**(5), 453–466.
38 R. Jin, Quantum sized, thiolate-protected gold nanoclusters, *Nanoscale*, 2010, **2**(3), 343–362.
39 K. Vangala, C. U. Pittman, D. Zhang, Y. Xin, K. B. Walters, E. Vasquez and K. Siriwardana, Simultaneous and Sequential Protein and Organothiol Interactions with Gold Nanoparticles, *J. Phys. Chem. C*, 2013, **117**(3), 1366–1374.
40 E. Casals, T. Pfaller, A. Duschl, G. J. Oostingh and V. Puntes, Time evolution of the nanoparticle protein corona, *ACS Nano*, 2010, **4**(7), 3623–3632.
41 L. Treuel, M. Malissek, J. S. Gebauer and R. Zellner, The influence of surface composition of nanoparticles on their interactions with serum albumin, *ChemPhysChem*, 2010, **11**(14), 3093–3099.
42 K. Vangala, F. Ameer, G. Salomon, V. Le, E. Lewis, L. Yu, D. Liu and D. Zhang, Studying Protein and Gold Nanoparticle Interaction Using Organothiols as Molecular Probes, *J. Phys. Chem. C*, 2012, **116**(5), 3645–3652.
43 L. Shang, S. Brandholt, F. Stockmar, V. Trouillet, M. Bruns and G. U. Nienhaus, Effect of protein adsorption on the fluorescence of ultrasmall gold nanoclusters, *Small*, 2012, **8**(5), 661–665.
44 J. R. Lakowicz, *Principles of fluorescence spectroscopy*, Springer, 2009, vol. 8.
45 P. J. Goutam, D. K. Singh and P. K. Iyer, Photoluminescence Quenching of Poly (3-hexylthiophene) by Carbon Nanotubes, *J. Phys. Chem. C*, 2012, **116**(14), 8196–8201.
46 A. Ahmad, T. Kurkina, K. Kern and K. Balasubramanian, Applications of the static quenching of rhodamine B by carbon nanotubes, *ChemPhysChem*, 2009, **10**(13), 2251–2255.
47 C. R. Carey, Y. Yu, M. Kuno and G. V. Hartland, Ultrafast Transient Absorption Measurements of Charge Carrier Dynamics in Single II–VI Nanowires, *J. Phys. Chem. C*, 2009, **113**(44), 19077–19081.
48 C. D. Grant, A. M. Schwartzberg, Y. Yang, S. Chen and J. Z. Zhang, Ultrafast study of electronic relaxation dynamics in Au_{11} nanoclusters, *Chem. Phys. Lett.*, 2004, **383**(1), 31–34.
49 S. Bhattacharyya, T. Sen and A. Patra, Host–Guest Energy Transfer: Semiconducting Polymer Nanoparticles and Au Nanoparticles, *J. Phys. Chem. C*, 2010, **114**(27), 11787–11795.
50 A. K. Singh, W. Lu, D. Senapati, S. A. Khan, Z. Fan, T. Senapati, T. Demeritte, L. Beqa and P. C. Ray, Long-Range Nanoparticle Surface-Energy-Transfer Ruler for Monitoring Photothermal Therapy Response, *Small*, 2011, **7**(17), 2517–2525.
51 P. K. Jain, W. Huang and M. A. El-Sayed, On the universal scaling behavior of the distance decay of plasmon coupling in metal nanoparticle pairs: a plasmon ruler equation, *Nano Lett.*, 2007, **7**(7), 2080–2088.
52 M. S. Devadas, K. Kwak, J.-W. Park, J.-H. Choi, C.-H. Jun, E. Sinn, G. Ramakrishna and D. Lee, Directional Electron Transfer in Chromophore-Labeled Quantum-Sized Au25 Clusters: Au25 as an Electron Donor, *J. Phys. Chem. Lett.*, 2010, **1**(9), 1497–1503.
53 G. Mandal, M. Bardhan and T. Ganguly, Occurrence of Förster Resonance Energy Transfer between Quantum Dots and Gold Nanoparticles in the Presence of a Biomolecule, *J. Phys. Chem. C*, 2011, **115**(43), 20840–20848.

